ACS Catalysis

pubs.acs.org/acscatalysis Research Article

Functional Plasticity of Methyltransferases in Anthracycline Biosynthesis: A Single Residue Reversal between Decarboxylation and Hydroxylation

Moli Sang, Qingyu Yang, Jiawei Guo, Peiyuan Feng, Yu Gao, Wencheng Ma, Shengying Li, Mikko Metsä-Ketelä, and Wei Zhang*

Cite This: ACS Catal. 2026, 16, 3522−3533 Read Online

ACCESS | Metrics & More | Article Recommendations | Supporting Information

ABSTRACT: The structurally homologous methyltransferases DnrK and RdmB catalyze mechanistically distinct and chemically atypical reactions during anthracycline biosynthesis. Through comprehensive functional analysis, we identified glutamic acid 299 as the critical molecular determinant responsible for their divergent catalytic behaviors. The substitution of E299 with a hydrophobic residue in DnrK was sufficient to confer RdmB-like hydroxylation activity, while the reverse mutation in RdmB introduced the decarboxylation capability. By systematically substituting E299 with residues of different properties, we successfully engineered a hybrid variant that integrates the functions of both parental enzymes capable of simultaneously producing four distinct types of anthracycline derivatives. These findings provide mechanistic insights into how subtle active-site modifications can drive the functional diversification of enzymes during evolution. Compounds **2** and **4** exhibited cytotoxicity against K-562 cells at the nanomolar level, demonstrating approximately 15-fold and 20-fold greater potency, respectively, compared to doxorubicin. This enhancement in antiproliferative activity underscores how strategic structural diversification of the anthracycline scaffold can improve pharmacological properties. Collectively, by elucidating the evolutionary strategy of DnrK and RdmB, our work provides potential next-generation anthracycline derivatives with optimized therapeutic profiles.

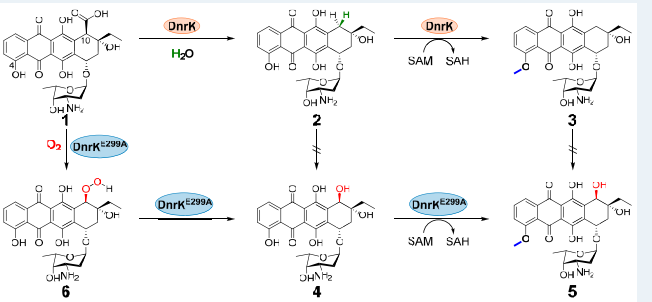

KEYWORDS: *anthracyclines, biosynthesis, methyltransferase, hydroxylation, enzymatic mechanism*

INTRODUCTION

Anthracycline-type natural products, such as doxorubicin, aclacinomycin A, and epirubicin, represent a major class of chemotherapeutic agents widely used in cancer treatment.[1−7] However, their clinical utility is often limited by associated side effects.[8,9] Consequently, significant efforts have been directed toward generating structurally modified anthracyclines with an improved therapeutic index.[5] Biosynthetically, anthracyclines are assembled by type II polyketide synthases and share a tetracyclic 7,8,9,10-tetrahydro-5,12-naphtacenequinone scaffold.[4,10] Their structural diversity and bioactivity are further expanded by tailoring enzymes—including hydroxylases, carboxylases, methyltransferases, and oxidases.[4,5] A deeper mechanistic understanding of these enzymes is therefore crucial for diversifying the anthracycline structures and optimizing their biological functions.

Notably, two atypical methyltransferase homologues—DnrK from *Streptomyces peucetius* and RdmB from *Streptomyces purpurascens*, are found with high protein sequence identity (53.4%) and structural similarity yet perform divergent catalytic functions in anthracycline biosynthesis.[11−14] DnrK is known as a bifunctional enzyme that catalyzes both the typical 4-*O*-methylation and an unusual 10-decarboxylation of 15-demethoxy-aclacinomycin T to generate 4-*O*-methyl-10-decarboxy-aclacinomycin T.[11,12] In contrast, RdmB was initially characterized as an aclacinomycin 10-hydroxylase, mediating the 10-decarboxylative hydroxylation of 15-demethoxy-ε-rhodomycin or 15-demethoxy-aclacinomycin T (Figure S1).[15,16] Recent work further revealed that RdmB also exhibits methyltransferase activity, catalyzing the methylation of 13-deoxycarminomycin to form 13-deoxydaunorubicin, a step in doxorubicin biosynthesis.[17] This conservation of methyltransferase activity, alongside their distinct transformations at C10 (decarboxylation versus hydroxylation),

Received: November 3, 2025
Revised: January 14, 2026
Accepted: January 14, 2026
Published: January 27, 2026

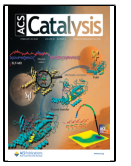

https://doi.org/10.1021/acscatal.5c07819
ACS Catal. 2026, 16, 3522−3533

Scheme 1. Reaction scheme mediated by DnrK and DnrK^{E299A}: 10-Carboxy-13-deoxycarminomycin (1), 13-Deoxycarminomycin (2), 13-Deoxydaunorubicin (3), 10-Hydroxyl-13-deoxydaunorubicin (4), 10-Hydroxyl-13-deoxycarminomycin (5), and Hydroperoxide Intermediate (6)

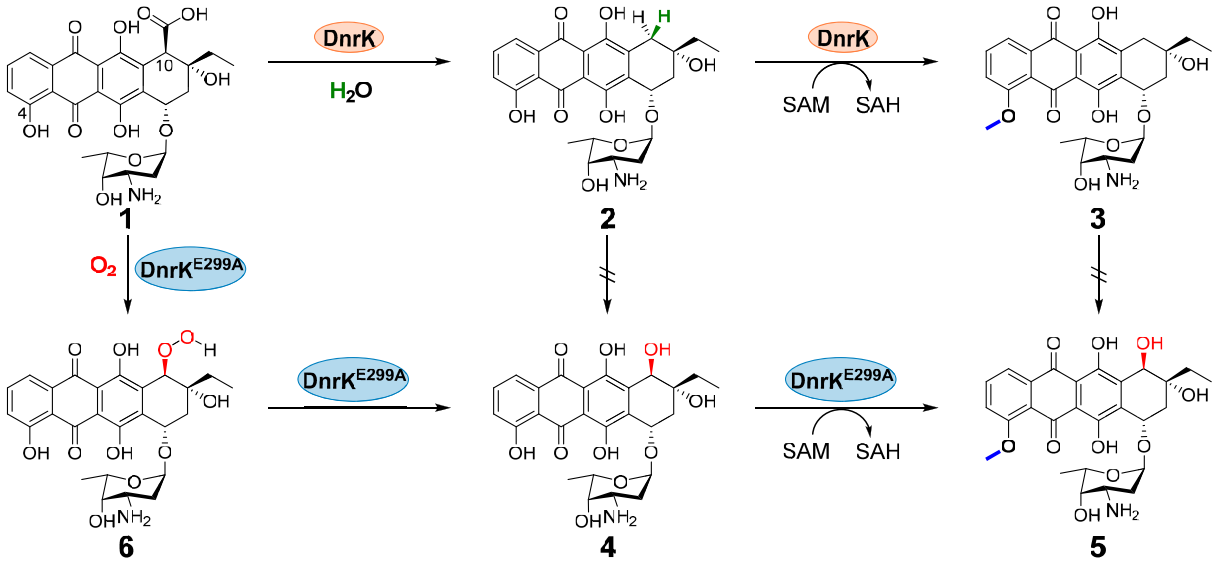

prompted us to investigate the molecular basis underlying their functional divergence.

In this study, by exploring the structural basis underlying the functional differences between DnrK and RdmB, we identified E299 as a key determinant, modulating their catalytic specificity and product profiles. Reciprocal mutations at this site were sufficient to interchange their enzymatic functions. Enzymatic reactions yielded four anthracyclines, among which antiproliferative screening identified compounds **2** and **4** as particularly effective against the K-562 cell line, indicating their potential as new anthracycline agents. This work shows that rational enzyme engineering will enable functional reprogramming and provide a strategy for designing optimized anthracycline derivatives with implications for advancing cancer therapeutics.

RESULTS

Discovery and Identification of E299 as a Function Modulator

DnrK is proposed to convert substrate 10-carboxy-13-deoxycarminomycin (**1**) into 13-deoxycarminomycin (**2**) via 10-decarboxylation, as well as into the 4-*O*-methylated product 13-deoxydaunorubicin (**3**) (Scheme 1). The gene encoding DnrK was amplified from the genome of a daunorubicin producer *Streptomyces coeruleorubidus*[18] and cloned onto the expression vector pET28a (Figure S2). Heterogeneous expressed in *Escherichia coli* BL21(DE3) yielded soluble protein (Figure S3A). Subsequently, in-vitro enzymatic assays were performed using DnrK in the presence of *S*-adenosylmethionine (SAM), with the natural substrate **1** isolated from the fermentation broth of of *dnrK* gene deletion mutant *S. coeruleorubidus*Δ*dnrK*.[17] As expected, two products **2** (m/z = 500.1921, M+H]$^+$, *calc.* 500.1915) together with **3** (m/z = 514.2078, [M + H]$^+$, *calc.* 514.2072) were observed by UPLC (Figures 1A-i and S4). These products were further confirmed by LC-HRMS and NMR spectroscopy (Figures S5 and S24–S33).

To investigate the catalytic mechanism of DnrK toward **1**, the X-ray crystal structure of DnrK in complex with *S*-adenosylhomocysteine (SAH) and product **3** was solved as homodimers at 1.3 Å resolution (PDB ID: 9LA8), due to the spontaneous decarboxylation of substrate **1** during the long crystallization time and the presence of protein-bounded SAM (Figure 1B and Table S2). Each subunit adopted the characteristic fold of Class I methyltransferases, featuring an *N*-terminal helical domain responsible for substrate recognition and dimerization, and a *C*-terminal Rossmann-like fold involved in substrate binding and catalysis.[19,20] The catalytic pocket contained product **3**, while SAH was bound to the conserved GxGxG motif located in a loop between the first β-sheet and an α-helix within the Rossmann fold, in close proximity to the product.[21]

The key residues directly involved in the methyl transfer reaction of DnrK had not been experimentally indentified.[14] Molecular docking of **1** into the DnrK structure using AutoDock Vina suggested that Y143 and N257 form hydrogen bonds (3.0 and 2.8 Å, respectively) with the C4-hydroxyl group of **1** (Figure 1C). The binding pose of docked substrate **1** is closely aligned with that of product **3** in the DnrK crystal structure, particularly within the core scaffold region. Key active-site residues involved in substrate interactions, such as R303, N257, and Y143, exhibit highly similar orientations in both models (Figure S6). Subsequently, the mutated proteins DnrK^{Y143A} and DnrK^{N257A} were purified, respectively (Figure S3B and S3C). Incubation of DnrK^{Y143A} with **2** in the presence of SAM retained the ability to produce methylated product **3**, whereas DnrK^{N257A} completely abolished the methylation activity (Figure S7). When compound **1** was used as the substrate, the DnrK^{N257A} mutant retained the ability to bind SAM (Figure S8B-ii). However, this mutant yielded only decarboxylated product **2**, with no methylated product detected (Figure 1A-ii). To further elucidate the role of N257, we constructed mutants (N257L, N257Q, and N257D) and incubated them individually with substrate **1** (Figure S9A). Consistent with the N257A mutant, all three variants produced only the decarboxylated product **2**, with no methylation

https://doi.org/10.1021/acscatal.5c07819
ACS Catal. 2026, 16, 3522−3533

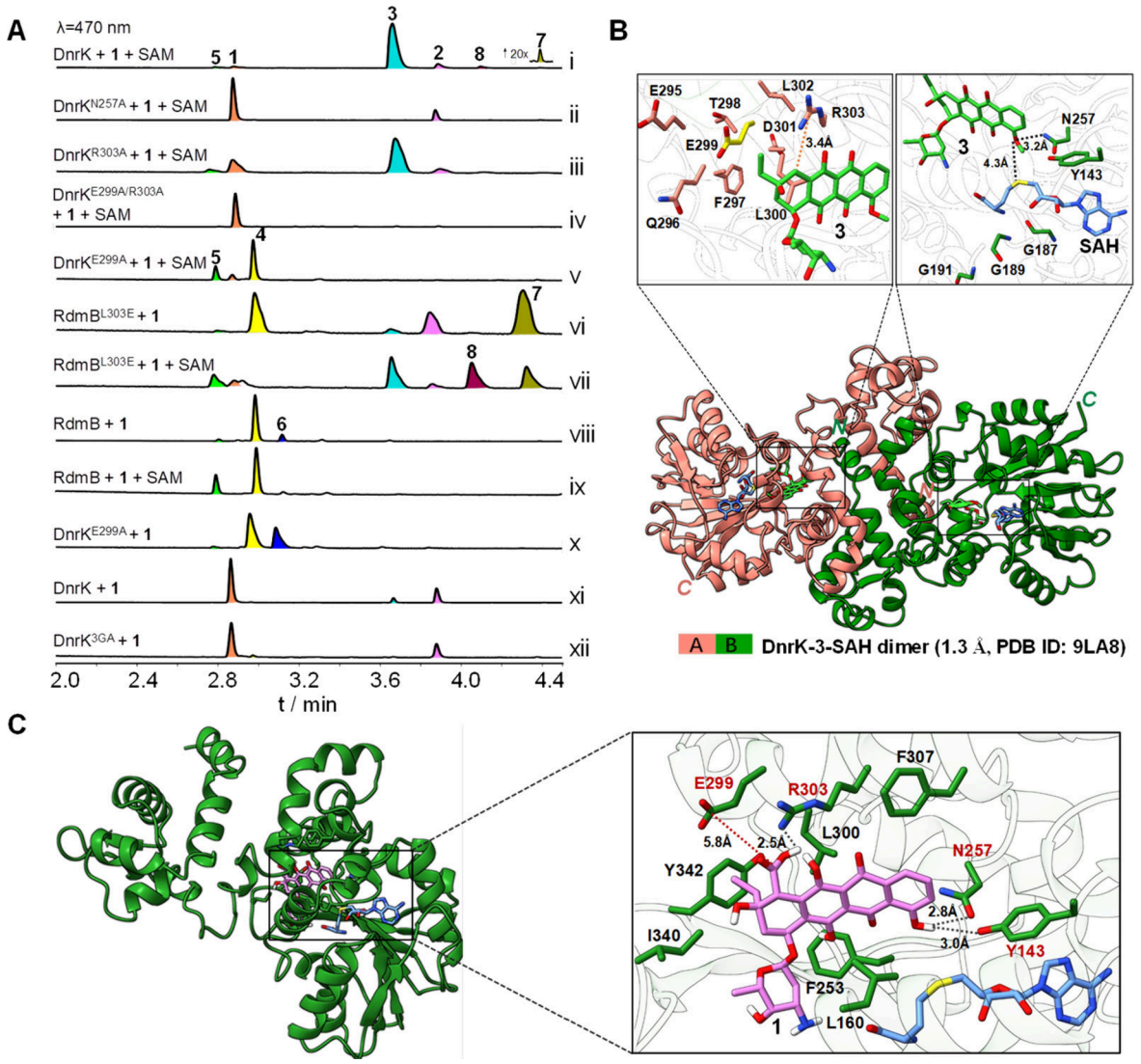

Figure 1. In-vitro enzymatic conversions of substrate **1** and the docking model with DnrK. (A) Comparative analysis of the enzymatic conversion of **1** catalyzed by DnrK and its mutants in vitro. (i) The conversion of **1** by DnrK in the presence of 1 mM SAM; (ii) The conversion of **1** by DnrK^{N257A} in the presence of 1 mM SAM; (iii) The conversion of **1** by DnrK^{R303A} with 1 mM SAM; (iv) The conversion of **1** by DnrK$^{R303A/E299A}$ with SAM; (v) The conversion of **1** by DnrK^{E299A} with SAM; (vi) The conversion of **1** by RdmB^{L303E} without SAM; (vii) The conversion of **1** by RdmB^{L303E} with SAM; (viii) The conversion of **1** by wild-type RdmB without SAM; (ix) The conversion of **1** by RdmB with SAM; (x) The conversion of **1** by DnrK^{E299A} without additional cofactor SAM; (xi) the conversion of **1** by DnrK without additional cofactor SAM; (xii) the conversion of **1** by DnrK^{3GA} without additional cofactor SAM. (B) 3D structure of DnrK bound with product **3** and SAH. The two monomers of DnrK are colored pink and cyan. The bound ligands of SAH and **3** are shown in the stick models in blue and green. The top box shows a zoomed-in view of the active site of DnrK with **3**. (C) The docking model of DnrK in complex with substrate **1** (purple). The box shows a close-up view of the active site of DnrK with docked **1**. In this view, the combined ribbon diagram and stick-ball model show the detailed interactions of DnrK with docked **1**. The hydrogen bonds interactions are shown as black dotted lines; The orange dashed line indicates the distance between the side chain carboxyl group of E299 residue and the carboxyl group of the substrate.

product **3** detected (Figure S9B). These results suggest the N257 plays a key role in the methyl transfer step, likely by maintaining the proper active-site geometry and stabilizing the transition state.[14,22,23]

We next sought to elucidate the structural basis for the decarboxylation activity of DnrK at the C10-carboxyl group of substrate **1**. Structural analysis revealed that the *N*-terminal α-16 helix is positioned in proximity to this group, with R303 forming a 2.5 Å hydrogen bond to the carboxylate moiety (Figure 1C). This arginine is conserved in the complex crystal structure of RdmB with **3** (PDB ID: 8KHJ), where it has been shown to facilitate decarboxylative hydroxylation by our group.[17] However, its mutation to alanine in DnrK (DnrK^{R303A}) did not abolish activity; both decarboxylated (**2**) and methylated (**3**) products were still detected by UPLC (Figure 1A-iii). This result implies that the decarboxylation mechanism in DnrK differs from that in RdmB, potentially contributing to their functional divergence.

Further sequence and structural alignment highlighted a key substitution within the α-16 helix: E299 in DnrK is replaced by a nonpolar leucine (L303) in RdmB. The acidic side chain of E299 is oriented toward the C10-carboxyl group of **1**, situated 5.8 Å away (Figures 2 and S10). Notably, the double mutant DnrK$^{R303A/E299A}$ lost all of the decarboxylation activity toward substrate **1** (Figure 1A-iv), indicating that both residues cooperatively contribute to C10-decarboxylation.

https://doi.org/10.1021/acscatal.5c07819
ACS Catal. 2026, 16, 3522−3533

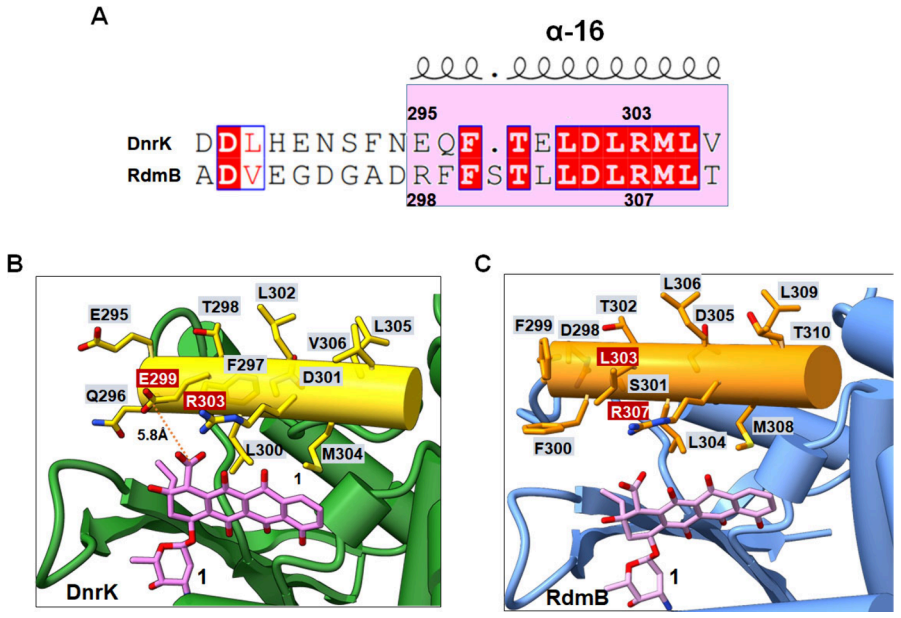

Figure 2. Sequence alignment and molecular docking analysis of DnrK and RdmB with substrate **1**. (A) Sequence alignment of the *N*-terminal α-16 helix between DnrK and RdmB. (B) View of the α-16 helix in DnrK represented by the yellow cylinder, highlighting key amino acid residues with a red background. (C) View of the α-16 helix in RdmB represented by the orange cylinder, highlighting key amino acid residues with a red background.

To probe the role of E299, we generated a series of site-directed mutants (Figure S11). UPLC and LC-HRMS analyses showed that the DnrK^{E299A} mutant abolished the formation of products **2** and **3** in the presence of SAM, but surprisingly generated a new product **4** (Figure 1A-v). The *m*/*z* value of **4** was found to be 16 Da more than that of **2** by LC-HRMS analyses (*m*/*z* = 500.1921 vs 516.1873, $[M + H]^+$; Figure S4), which was subsequent identified as 10-hydroxyl-13-deoxy-carminomycin by 1D and 2D NMR (Figures S5 and S34−38). These results demonstrated the mutation of E299A introduced the 10-hydroxylation activity to DnrK. Further control experiments showed that neither **2** nor **3** could be hydroxylated by DnrK^{E299A} (Figure S12), indicating the inert CH_2 group cannot be activated by DnrK^{E299A} and the hydroxylation proceeds directly following the formation of the anion resulted from 10-decarboxylation within the catalytic center.[16] Additionally, DnrK^{E299A} was capable of methylating **4** to yield compound **5** (*m*/*z* 530.2028, $[M + H]^+$), as confirmed by UPLC and LC-HRMS (Figure 1A-v, Figure S5 and S39−S43). It is noteworthy that **5** and the demethylated product **4** can be also detected as trace amount products by LC-HRMS in wild-type DnrK reactions, which may be byproducts arising from a moonlighting activity of DnrK (Figures 1A-i and S13).

To test the transferability of this functional switch, we constructed reciprocal mutant RdmB^{L303E}. In addition to producing native **4** and **5** when incubated with substrate **1** without the addition of SAM, this variant also generated the 10-decarboxylated product **2** and further methylated **3** (Figure 1A-vi). Two additional products **7** and **8** were detected and identified as anthracycline derivatives based on their characteristic UV−vis spectra (Figures 1A-vii and S14A). LC-HRMS analysis suggested **7** (*m*/*z* = 482.1807 $[M + H]^+$; *calc.* 482.1809) arises from a C9−C10 elimination of **2**, and **8** (*m*/*z* = 496.1957 $[M + H]^+$; *calc.* 496.1966) is the methylated derivative of **7** (Figure S14B). These products are not observed with wild-type RdmB (Figure 1A-viii, ix) but are presented in trace amounts in the product profile of wild-type DnrK (Figure 1A-i). Thus, the L303E mutation confers DnrK-like decarboxylation activity on RdmB.

To systematically probe the functional role of E299 of DnrK, we engineered a number of variants by substituting this residue with amino acids of distinct physicochemical properties: hydrophobic leucine (L), hydrophilic aspartic acid (D), glutamine (Q), and lysine (K) (Figure S11). While DnrK^{E299L} and DnrK^{E299A} showed nearly identical activity profiles, and DnrK^{E299D} behaved similarly to the wild-type enzyme, a remarkable functional divergence was observed with DnrK^{E299K} and DnrK^{E299Q} (Figure 3C). These two mutants functioned as true catalytic hybrids, simultaneously producing both decarboxylated (**2**) and hydroxylated (**4**) products, along with their corresponding methylated derivatives (**3** and **5**). This result demonstrates that the residue at position 299 serves as a functional modulator capable of tuning DnrK toward decarboxylation, hydroxylation, or a hybrid functional profile, effectively integrating the catalytic features of both DnrK and RdmB into a single enzyme.

In order to gain deeper insights into the structural basis for the hydroxylation activity of DnrK^{E299A}, we tried to solve its crystal structure in complex with substrate **1** and SAM. As a result, the DnrK^{E299A}-**5**-SAH ternary complex structure was solved at a resolution of 1.70 Å (PDB ID: 9LAC) and revealed a homodimer with SAH bound in the active site (Figure 3A and Table S2). The overall tertiary structure of DnrK^{E299A} closely resembled that of DnrK^{WT} with a root-mean-square deviation (RMSD) of 0.42 Å over all Cα atoms, and the position of products **3** and **5** within the catalytic pocket was similar. No significant alterations were observed in the residues interacting with the C4 and C10 positions and other amino acids on the α-16 helix, aside from the E299A substitution itself. This finding underscores that the substitution of a single residue at position 299 is reprogramming the function and product profile of DnrK.

https://doi.org/10.1021/acscatal.5c07819
ACS Catal. 2026, 16, 3522−3533

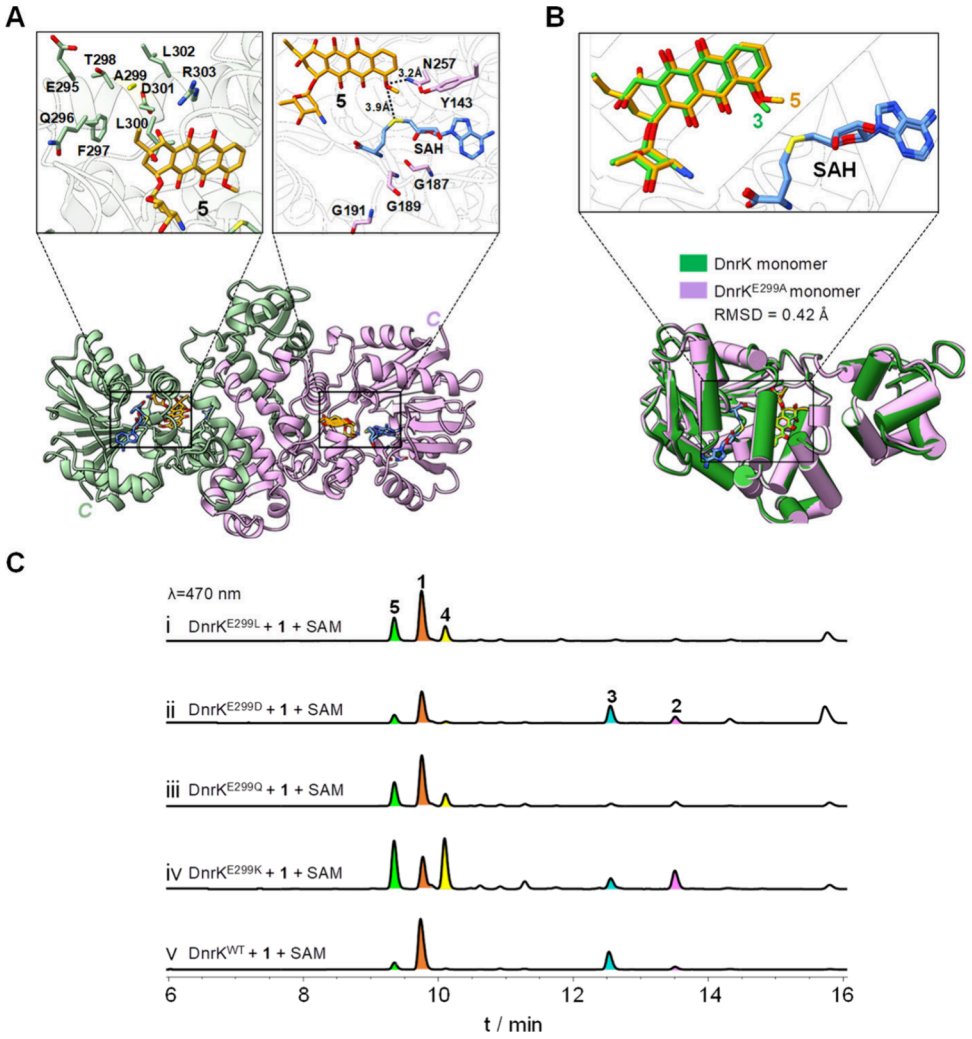

Figure 3. Ternary structure complexes of DnrK^{E299A}-**5**-SAH and the enzymatic conversion of **1** catalyzed by DnrK^{E299} mutants. (A) 3D structure of DnrK^{E299A} bound with 10-hydroxylation product **5** and SAH. The two monomers of DnrK^{E299A} are colored sea green and lilac. The bound ligands of SAH and **5** are shown in the stick models by cornflower blue and orange, respectively. The top box shows a zoomed-in view of the active site of DnrK^{E299A} with **5**. (B) Structural comparison of monomeric DnrK-**3**-SAH and monomeric DnrK^{E299A}-**5**-SAH, respectively. The box shows a close-up view of the binding of **3** or **5** in the active pockets of DnrK and DnrK^{E299A}. (C) HPLC analysis of the conversion of **1** catalyzed by DnrK and its mutants; (i) DnrK^{E299L}, (ii) DnrK^{E299D}, (iii) DnrK^{E299Q}, (iv) DnrK^{E299K}, and (v) DnrK^{WT} in the presence of SAM, respectively.

Role of SAM for Different Functions of DnrK

The product profile of DnrK^{E299A} was found to closely resemble that of wild-type RdmB, which catalyzes the conversion of substrate **1** to products **4** and **5** in the presence of SAM.[17] Previous studies have shown that in the absence of SAM, RdmB first forms a peroxide intermediate **6**, which subsequently undergoes homolytic O−O bond cleavage to yield **4**.[11,17] Consistent with this mechanism, we detected the formation of **6** (m/z = 532.1822 $[M + H]^+$; *calc.* 532.1813) in the DnrK^{E299A} reaction mixture even without exogenous SAM and reductant, as confirmed by UPLC and LC-HRMS analyses (Figures 1A-ix and S15). This result further confirms that the E299 mutation effectively converts DnrK to an RdmB-like enzyme.

Differently, in the absence of exogenous SAM, the decarboxylated product **2** was the predominant species formed by DnrK, accompanied only by a trace amount of the methylated product **3** (Figure 1A-x). The formation of **3** was attributed to residual SAM that copurified with the enzyme, as confirmed by the detection of SAM in the heat-denatured supernatant of DnrK using HPLC and LC-HRMS analysis (Figure S8B-i). These observations indicate that the decarboxylation activity of DnrK is independent of exogenously supplied SAM or its analogs.

To test this hypothesis, we mutated the three conserved glycine residues within the SAM-binding motif (GxGxG) of DnrK to alanine, generating the triple mutant DnrK^{3GA}, which fails to bind the SAM (Figures S3 and S8B-iii). When DnrK^{3GA} was incubated with substrate **1** in vitro, the decarboxylated product **2** accumulated in a time-dependent manner. This result confirmed that the decarboxylation activity of DnrK is independent of SAM binding (Figures 1A-xi and S16). The catalytic efficiency was further supported by competitive inhibition assays: addition of SAH (200 μM) or sinefungin (200 μM)[24,25] only marginally attenuated the consumption of **1** and the formation of **2**, consistent with results from the DnrK^{3GA} mutant and reactions lacking exogenous SAM (Figure S17). Circular dichroism (CD) spectra confirmed that the overall structure and conformation of DnrK^{3GA} remained largely similar to those of the wild-type enzyme

https://doi.org/10.1021/acscatal.5c07819
ACS Catal. 2026, 16, 3522−3533

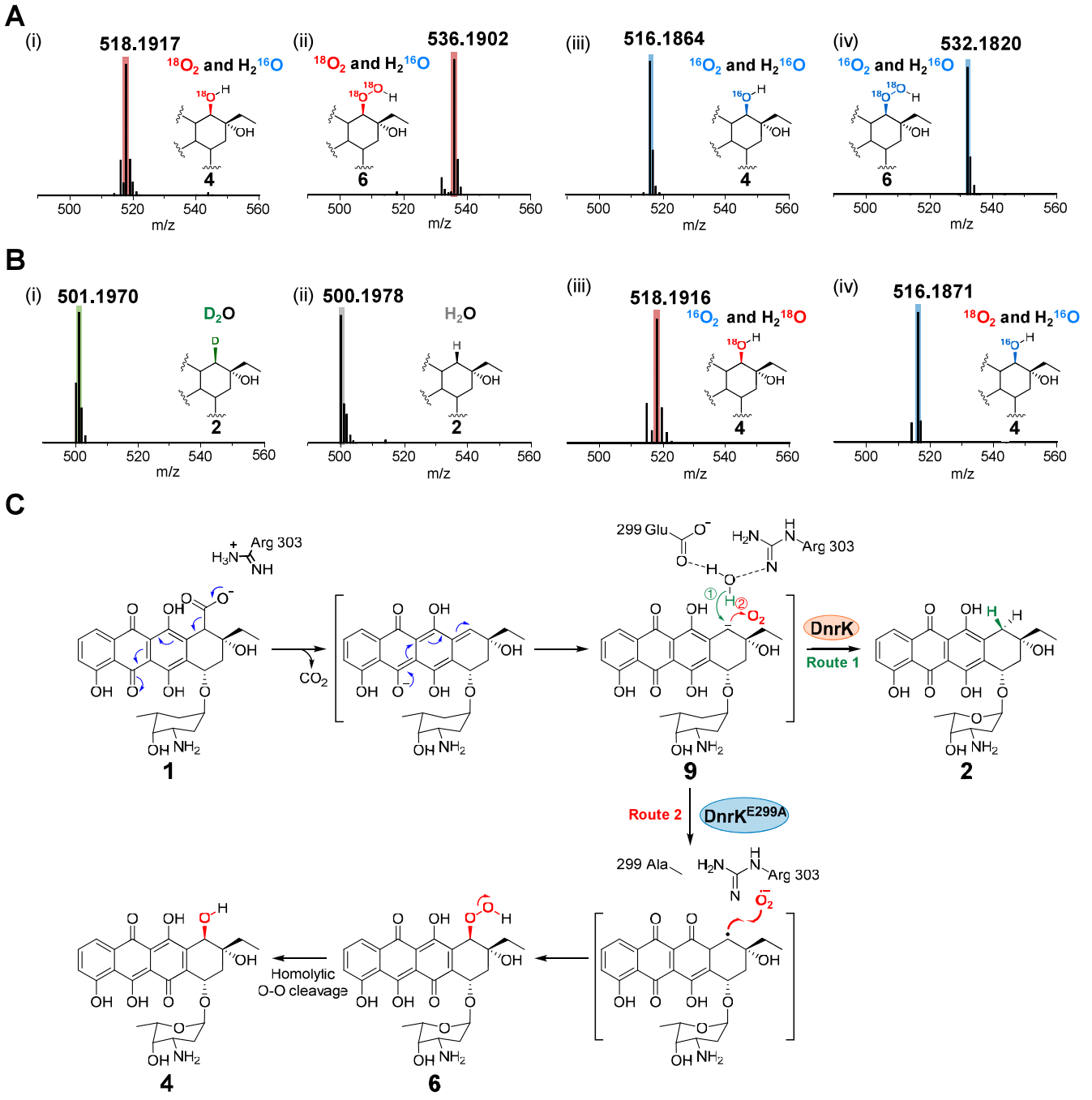

Figure 4. Isotopic labeling investigation of DnrK and its mutants. (A) LC-HRMS of **4** (i) and **6** (ii) delivered by $DnrK^{E299A}$ in $^{18}O_2$ with $H_2{}^{16}O$; LC-HRMS of **4** (iii) and **6** (iv) delivered by $DnrK^{E299A}$ in $^{16}O_2$ with $H_2{}^{16}O$. (B) LC-HRMS analysis of **2** produced by DnrK in D_2O (i) and H_2O (ii); LC-HRMS analysis of **4** produced by DnrK a mixture of (iii) $^{16}O_2$ and $H_2{}^{18}O$, and (iv) $^{18}O_2$ and $H_2{}^{16}O$. (C) Proposed catalytic mechanism of DnrK and $DnrK^{E299A}$.

(Figure S18), indicating that the loss of methylation activity stems from the specific disruption of SAM binding rather than overall structural changes. Collectively, these results establish that DnrK functions as a cofactor-less enzyme, capable of catalyzing both decarboxylation and hydroxylation independently of SAM or its analogues.

Oxygen Origins of C-10 Hydroxy Group

To elucidate the catalytic differences underlying the divergent product profiles of $DnrK^{WT}$ and $DnrK^{E299A}$, we performed isotope labeling experiments. When the $DnrK^{E299A}$ was reacted under an $^{18}O_2$ atmosphere, the masses of **4** and **6** were increased by 2 and 4 Da, respectively (Figure 4A-i, ii). However, when the reaction was carried out in $H_2{}^{18}O$ buffer, no mass shift was observed for either product (Figure 4A-iii, iv). Accordingly, when E299 is replaced by the hydrophobic residue A, the C-10 hydroxy oxygen atom in **4** and **6** were originated exclusively from O_2.

On the other side, when the reaction of $DnrK^{WT}$ was performed in D_2O buffer, a 1 Da increase in the mass of product **2** was observed by LC-HRMS analysis ($[M + H]^+$, 501.1967 vs. 500.1978 in H_2O; Figure 4B-i, ii. We also investigated the oxygen source of the minor product **4** that was

https://doi.org/10.1021/acscatal.5c07819
ACS Catal. 2026, 16, 3522−3533

derived from the moonlighting activity of DnrK^{WT}. Interestingly, only when the reaction of DnrK^{WT} was carried out in $H_2{}^{18}O$ buffer, the mass of **4** increased by 2 Da ($[M + H]^+$, 518.1916 *vs.* 516.1864 in $H_2{}^{16}O$; Figure 4B-iii). The introduction of $^{18}O_2$ atmosphere has no effect of the molecular mass of compound **4** by LC-HRMS analysis (Figure 4B-iv). These results indicate that the C-10 hydroxy oxygen in the byproduction of **4** by DnrK^{WT} is formed during the water-mediated decarboxylation.

Similarly, when E299 is replaced by the hydrophobic residue L, the C-10 hydroxy oxygen atom in **4** and **6** were originated from O_2 (Figure S19A), whereas DnrK^{E299D} behaves like the wild type, utilizing water as the oxygen source (Figure S19B). Interestingly, DnrK^{E299Q} and DnrK$^{E299\ K}$ incorporated oxygen of C-10 hydroxy from both O_2 and H_2O into products **4** and **5** (Figures S19C and S19D), consistent with their hybrid catalytic activities.

Based on these results and the reported substrate-assisted catalytic logic of cofactor-independent oxygenases,[26−29] we propose the catalytic mechanism of DnrK. Specifically, after substrate **1** binds to the active site, decarboxylation occurs via the action of R303 and E299, generating a carbanion at C10 of intermediate **9**. The hydrophilic microenvironment maintained by E299 helps anchor and orient a water molecule that acts as a direct proton source, rapidly quenching **9** to yield product **2** (Route 1). In contrast, substitution of E299 with a nonpolar residue (A or L) disrupts this potential hydrophilic network, resulting in a more hydrophobic pocket. Under these conditions, following a substrate-assisted O_2 activation mechanism analogous to that observed in HOD and DpgC,[30,31] single-electron transfer from anion **9** to O_2 generates a substrate−superoxide anion radical pair, which leads to the formation the peroxide intermediate **6** (Route 2). Subsequently, **6** is then converted to the final hydroxylated product **4**, a transformation that may proceed via either single-electron reductive cleavage or homolytic cleavage of the O−O bond (Figure 4C).

Antiproliferative Screening

To evaluate the bioactivities of compounds **2**−**5**, each was purified through large-scale enzymatic reactions and screened for antiproliferative effects across a panel of 16 human cancer cell lines. The results indicated that all four compounds exhibited cytotoxic potential against most of the tested cell lines (Table S3). Notably, compounds **2** and **4** displayed potent and selective antiproliferative activity against the K-562 cell line, with IC_{50} values of 0.06 ± 0.01 and 0.05 ± 0.01 μM, respectively (Table S4 and Figure S20). These IC_{50} values were substantially lower than that of doxorubicin hydrochloride (IC_{50} = 0.89 ± 0.11 μM), highlighting their enhanced efficacy. Ongoing studies are focused on elucidating the structure−activity relationship and mechanism of action of compounds **2** and **4**, which may provide valuable insights for the development of novel anthracycline-based anticancer agents.

DISCUSSION

Two methyltransferases, DnrK and RdmB, which participate in anthracycline biosynthesis, exhibit unusual catalytic functions despite sharing high sequence and structural similarity.[11,13,14,32] In particular, DnrK from the doxorubicin pathway not only performs the typical 4-*O*-methylation but also catalyzes 10-decarboxylation, while its close homologue RdmB from the rhodomycin pathway mediates 10-hydroxylation in addition to 4-*O*-methylation.

In this study, integrated 3D structural analysis and site-directed mutagenesis showed that the *N*-terminal α-16 helix lies in close proximity to the carboxyl group of substrate **1**. Strikingly, a single residue, E299, was identified as the key determinant responsible for switching catalytic specificity between these two atypical methyltransferases. Replacing E299 with a nonpolar residue (A or L) endowed DnrK with RdmB-like 10-hydroxylation activity, whereas introducing E at the corresponding site in RdmB (RdmB^{L303E}) conferred DnrK-like 10-decarboxylation activity.

Comprehensive sequential alignment revealed that glutamate (E299) in DnrK is a distinctive feature, which is replaced by a hydrophobic residue (L or V) in homologues such as ZamB, CalMB, TamK, and EamK (Figure S21). ZamB and CalMB are reported to catalyze the 10-hydroxylation of aclacinomycin T, whereas EamK and TamK catalyze the 10-decarboxylation the same substrate.[12,33] To experimentally probe the effect of this residue substitution, we expressed and purified codon-optimized versions of all four proteins, along with relevant mutants, in *Escherichia coli* BL21(DE3), and tested their activities with substrate **1** (Figure S22). As a result, two decarboxylases TamK and EamK exclusively catalyzed the formation of decarboxylated product **2**, while mutants TamK^{V311E} and EamK^{V314E} showed significantly reduced or abolished activity, indicating that the valine at this position is crucial for the catalytic function of them. However, under the same reaction conditions, the hydroxylases ZamB and CalMB produced no detectable products with substrate **1**, possibly due to substrate incompatibility (Figure S23). This result precluded further investigations of the mutations at the 299-equivalent site. It is noteworthy that our prior study achieved non-natural C-10 hydroxylation in a DnrK mutant through insertion of Ser297, which changed phenylalanine F296 recognition and obstructed a surface solvent channel.[11]

Isotopic labeling studies indicated that the oxygen atom incorporated into the 10-OH group was found to derive from molecular O_2 in hydrophobic E299 substitution mutants, whereas it originated from water in the corresponding hydrophilic variants of DnrK. Two hydrophilic residues, E299 and R303, both situated in the *N*-terminal α-16 helix, appear to coordinate water molecules and facilitate hydrogen-bonding networks essential for proton transfer, underscoring the important contribution of water-mediated hydrogen bonding in enzymatic catalysis. Furthermore, a growing group of enzymes structurally resembling methyltransferases catalyze diverse reactions beyond methylation, such as cyclopropanation (C10Q),[34] pericyclization (LepI),[35,36] deformylation and epoxidation (TnmJ),[37] as well as dehydration and spirocyclization (SlnM).[38]

Additionally, mutation of the SAM-binding motif (GxGxG) in DnrK specifically abolished methylation without affecting the decarboxylation or hydroxylation activities. This finding aligns with the growing recognition that enzymes within the methyltransferase superfamily can function independently of their canonical cofactor. Examples include SpnF and SpnL, which catalyze intramolecular [4 + 2]-cycloaddition and cyclization during spinosyn biosynthesis in the presence of SAH,[39] AlpH, which catalyzes a hydrazine-carbonyl condensation and ring closure in kinamycin biosynthesis without any cofactor,[40] and AdxI, which mediates pericyclic reactions in pyridoxatin biosynthesis.[41] The functional characterization

https://doi.org/10.1021/acscatal.5c07819
ACS Catal. 2026, 16, 3522−3533

of DnrK thus offers novel insights into the catalytic versatility of SAM-dependent methyltransferases and highlights the underappreciated role of cofactor-independent methyltransferase-like enzymes.

These findings also inform structure−activity relationship studies of anthracyclines. The notable antiproliferative effects of compounds **2** and **4** against the K-562 cell line suggest promising directions for the development of novel anthracycline-based agents. This work lays a foundation for the discovery and optimization of new anthracycline derivatives, with potential implications for advancing cancer therapeutics.

CONCLUSIONS

In conclusion, this work systematically reveals the key molecular determinant underlying the functional divergence between homologous methyltransferases DnrK and RdmB in anthracycline biosynthesis. Mechanistic and functional analyses identified the active-site residue E299 as the key modulator of the function switch between their decarboxylation and hydroxylation pathways. By engineering this site, we swapped their catalytic functions and created a dual-function variant that simultaneously produces four anthracycline compounds. Among these, compounds **2** and **4** showed markedly superior antiproliferative activity against K-562 cells over doxorubicin. These findings highlight the potential of rational anthracycline scaffold modification to enhance bioactivity and illustrate the utility of structure-guided enzyme engineering in generating valuable drug candidates.

MATERIALS AND METHODS

Materials

The antibiotics used in this study were procured from Solarbio (Beijing, China). All DNA restriction enzymes were purchased from Thermo Fisher Scientific (PA, USA). DNA amplification was carried out using 2× Phanta Max Master Mix from Vazyme (Nanjing, China). Reagents for plasmid mini preparation and DNA gel purification were obtained from Omega Biotek, Inc. (GA, USA). The substrate, 10-carboxy-13-deoxycarminomycin (**1**), was extracted from *S. coeruleorubidus*Δ*dnrK*. Compounds **2**−**5** were generated via biochemical conversions. *S*-adenosyl-L-methionine (SAM) and *S*-adenosyl-L-homocysteine (SAH) were acquired from Aladdin (Shanghai, China), while Sinefungin was sourced from Psaitong Biotechnology Co., Ltd. (Beijing, China). Protein purification was performed using Ni-NTA Sefinose resin from Sangon Biotech (Shanghai, China). The premixed gel solution for SDS PAGE was supplied by MDBio (Qingdao, China). Custom oligonucleotide primers and DNA sequencing services were provided by Sangon Biotech (Shanghai, China). Gene synthesis was commissioned by the Beijing Genomics Institute (Shenzhen, China). All solvents for compound isolation and purification were purchased from Sinopharm (Shanghai, China).

Analytical Procedures

The protein sequence alignments were made on T-Coffee[42] and ESPript3.[43] The biosynthetic gene clusters of *S. coeruleorubidus* were predicted using antiSMASH bacterial version (https://secondarymetabolites.org/).[44] NMR data was processed using MestReNova 9.0. All HPLC (DIONEX Ultimate 3000 instrument) analyses were performed using a YMC Triart C18 (4.6 × 250 mm, 5 μm, UV detection at 470 nm) column with a biphasic solvent system of acetonitrile−0.1% formic acid (solvent B) and water (solvent A) at a flow rate of 1.0 mL/min. All UPLC (ACQuity-H-class, Waters) analyses were performed using a YMC Triart C18 (2.1 × 100 mm, 1.9 μm, UV detection at 470 nm) column with a biphasic solvent system of acetonitrile−0.1% formic acid (solvent B) and water (solvent A) at a flow rate of 0.4 mL/min. LC-HRMS was performed by using a Bruker Impact HD High Resolution Q-TOF mass spectrometer.

Protein Expression Plasmid Construction

The DNA sequence encoding *dnrK* were amplified from the gDNA of *S. coeruleorubidus* using the primer pair of dnrK-F/dnrK-R. The purified DNA fragments were ligated into *Nde*I/*Hind*III-digested pET28a (+) with his^{6} at the *N*-terminus using the ClonExpress Ultra One Step Cloning Kit, and transformed into *E. coli* DH5α for plasmid amplification. The recombinant plasmid was verified by DNA sequencing, and the correct plasmids were transformed into *E. coli* BL21(DE3) for protein overexpression. The site-specific mutations of DnrK were constructed by site-directed PCR using pET28a-dnrK as template using primer pairs of dnrK^{3GA}-F/dnrK^{3GA}-R, dnrK^{Y143A}-F/dnrK^{Y143A}-R, dnrK^{N257A}-F/dnrK^{N257A}-R, dnrK^{N257L}-F/dnrK^{N257L}-R, dnrK^{N257Q}-F/dnrK^{N257Q}-R, dnrK^{N257D}-F/dnrK^{N257D}-R, dnrK^{R303A}-F/dnrK^{R303A}-R, dnrK^{E299A}-F/dnrK^{E299A}-R, dnrK$^{E299A/R303A}$-F/dnrK$^{E299A/R303A}$-R, dnrK^{E299L}-F/dnrK^{E299L}-R, dnrK^{E299D}-F/dnrK^{E299D}-R, dnrK^{E299Q}-F/dnrK^{E299Q}-R, dnrK^{E299K}-F/dnrK^{E299K}-R. The specific PCR product was purified with the Omega Gel Extraction Kit following the protocol provided by the supplier and subsequently introduced into *E. coli* DH5α cells for plasmid multiplication. The obtained recombinant plasmids were confirmed by DNA sequencing, and the accurately sequenced plasmids were then individually transformed into *E. coli* BL21(DE3) cells for the purpose of overexpressing the respective proteins.

Heterologous Expression and Purification of Recombinant Proteins

Each protein expression strain was grown overnight in LB medium with 50 μg/mL kanamycin at 37 °C and 220 rpm. The culture was then grown in 2 L of LB at 37 °C until the OD_{600} reached 0.6−0.8, and protein expression was induced with 0.2 mM IPTG at 16 °C for 16−20 h. The cells were harvested by centrifugation and stored at −80 °C until purification. The following steps were performed on ice. The cell pellets were resuspended in lysis buffer (50 mM NaH_2PO_4, 300 mM NaCl, 10 mM imidazole, 10% glycerol, pH 8.0) and then lysed using a high-pressure homogenizer. The lysate was centrifuged at 10 000 rpm at 4 °C for 60 min. The supernatant was collected and applied to the His-select nickel affinity column. After washing the unbound proteins with wash buffer (50 mM NaH_2PO_4, 300 mM NaCl, 20 mM imidazole, and 10% glycerol, pH 8.0), the target protein was eluted with elution buffer (50 mM NaH_2PO_4, 300 mM NaCl, 250 mM imidazole, and 10% glycerol, pH 8.0) and analyzed by SDS-PAGE. Subsequently, the eluted fractions were desalted using a PD-10 desalting column (GE Healthcare). The desired protein was finally stored in a storage buffer (50 mM NaH_2PO_4, 100 mM NaCl, and 10% glycerol, pH 7.4). Protein aliquots were stored at −80 °C until use. For crystallization of DnrK and DnrK^{E299A}, the eluted sample was applied to size-exclusion chromatography using the ÄKTA pure 25 system (GE) mount with Superdex 200 pg 16/600 column and equilibrated by buffer (20 mM Tris pH 8.0 and 150 mM NaCl) for further purification. Purified proteins were collected and concentrated to 13 mg/mL (DnrK) and 8 mg/mL (DnrK^{E299A}) in an Amicon Ultra-15 30 K device (Millipore) and stored at −80 °C.

In-Vitro Biochemical Assays and Product Detection

Unless stated otherwise, all enzymatic assays were carried out in a total volume of 100 μL in the desalting buffer (50 mM NaH_2PO_4, 300 mM NaCl, 10% glycerol, pH 7.4) at 30 °C, and the boiled enzymes were used as a negative control. For DnrK-mediated reaction, 0.1 mM of substrates was incubated with 2 μM of DnrK with or without 1 mM of SAM at 30 °C for 2 h. To analyze the activity of DnrK mutants, DnrK was replaced by its mutants (DnrK^{3GA}/DnrK^{N257A}/DnrK^{N257L}/DnrK^{N257Q}/DnrK^{N257D}/DnrK^{R303A}/DnrK^{Y143A}/DnrK^{E299A}/DnrK$^{E299A/R303A}$) in the above reaction system. The above reactions were quenched by mixing with 200 μL of methanol to precipitate the proteins. The metamorphic proteins were removed by centrifugation at 14 000*g* for 10 min, and the supernatants were analyzed with UPLC or LC-HRMS using gradient elution programs. Water-0.1% FA (solvent A) and acetonitrile−0.1% FA (solvent B) were used as the mobile phases. The UPLC program: 0−0.5 min, 20% B in A; 0.5−5 min, 20%−90% B in A; 5−5.1 min 90%−100% B in A; 5.1−5.6 min

https://doi.org/10.1021/acscatal.5c07819
ACS Catal. 2026, 16, 3522−3533

100% B; 5.6−5.7 min 100%−20% B in A; and 5.7−6.5 min 20% B in A at a flow rate of 0.4 mL/min, UV 470 nm. LC-HRMS program: 0−2 min, 20% B in A; 2−20 min, 20%−80% B in A; 20−20.5 min, 80%−100% B in A; 20.5−22 min, 100% B; 22−22.5 min, 100%−20% B in A; and 22.5−25 min, 20% B in A at a flow rate of 1 mL/min, UV 470 nm.

The reaction systems and conditions for the DnrK E299 mutants and DnrK homologous proteins (ZamB, CalMB, EamK, and TamK) with substrate **1** are identical to those for wild-type DnrK. The detection procedures of the reaction product are consistent with the LC-HRMS conditions.

Isolation of the Compounds 2−5

To identify the structure of **2**, an 80-mL-total-volume enzymatic reaction was performed in desalting buffer containing 0.25 mM of **1** and 10 μM of DnrK^{3GA}. After incubation at 30 °C for 4 h, 160 mL of methanol was used to quench the reaction. Compound **2** (2 mg) was purified from the concentrated reaction mixture by semipreparative HPLC using 50% ACN in H_2O (0.1% FA) at a flow rate of 3 mL/min.

To identify the structure of **3**, a 50-mL-total-volume enzymatic reaction were performed in desalting buffer containing 0.5 mM of **1**, 1 mM of SAM and 10 μM of DnrK. After incubation at 30 °C for 4 h, 100 mL methanol was used to quench the reaction. Compound **3** (3 mg) was purified from the concentrated reaction mixture by semipreparative HPLC using 45% ACN in H_2O (0.1% FA) at a flow rate of 3 mL/min.

To get sufficient amout of **4**, a 200-mL-total-volume large-scale enzymatic reaction was performed in desalting buffer containing 0.5 mM of **1** and 10 μM of DnrK^{E299A}. After incubation at 30 °C for 2 h, 400 mL of methanol was added to quench the reaction. Compound **4** (5 mg) was purified from the concentrated reaction mixture by semipreparative HPLC using 24% ACN in H_2O (0.1% FA) at a flow rate of 3 mL/min.

To identify the structure of **5**, a 50-mL-total-volume enzymatic reaction was performed in desalting buffer containing 0.5 mM of **4**, 10 μM of DnrK, and 1 mM of SAM. After incubation at 30 °C for 2 h, 100 mL methanol was added to quench the reaction. Compound **5** (2 mg) was purified from the concentrated reaction mixture by semipreparative HPLC using 26% ACN in H_2O (0.1% FA) at a flow rate of 3 mL/min.

The Confirmation of SAM Presence in DnrK^{WT}, DnrK^{N257A}, and DnrK^{3GA}

300 μM concentration of DnrK^{WT}, DnrK^{N257A}, and DnrK^{3GA} in 30 μL of storage buffer was denatured by heating at 100 °C for 10 min, respectively. 1 mM of SAM in water was heated at 100 °C for 10 min as a positive control. Then, the solutions were centrifuged at 14 000*g* for 10 min. The supernatants were analyzed by LC-HRMS with a linear gradient of 5%−60% ACN-H_2O with 5 mM ammonium acetate for 25 min at a flow rate of 1 mL/min. UV detection was performed at 260 nm.

Time-Dependent Conversion Experiments of 1 by DnrK^{3GA}

A 500 μL reaction mixture containing 100 μM of **1** with 2 μM of DnrK^{3GA} in desalting buffer was incubated at 30 °C. The time points for reactions were set at 0, 1, 2, 4, 6 h, respectively. When each reaction reached the reaction time point, the reaction mixture was terminated with 200 μL of methanol. After centrifuged at 14 000*g* for 10 min, the supernatants were analyzed by UPLC, UV 470 nm.

Crystallization, Data Collection, and Structure Determination

Purified DnrK or DnrK^{E299A} proteins were mixed with **1** (100 mM stock in DMSO) and SAM (1 M stock in buffer) to a 1:5:5 molar stoichiometry of protein:**1**:SAM. Crystals were obtained by utilizing the sitting drop vapor diffusion method in a 1:1 ratio with the crystallization condition. The cocomplex crystals of DnrK with **3** were grown in the precipitant solution of 0.1 M of Bis-Tris (pH 5.5), 2.0 M of ammonium sulfate and the co-complex crystals of DnrK^{E299A} with **5** were grown in the precipitant solution of 0.1 M BIS-TRIS (pH 6.5), 2.0 M ammonium sulfate. Crystals were supplemented with cryoprotectants containing the reservoir contents plus 20% ethylene glycol and flash-frozen in liquid nitrogen. Diffraction data of both DnrK-**3**-SAH and DnrK^{E299A}-**5**-SAH complex crystals was collected at 100 K on beamline BL18U at the Shanghai Synchrotron Radiation Facility (SSRF) and processed using the HKL3000 program.[45]

The structure of DnrK-**3**-SAH was solved by molecular replacement with the program Phaser,[46] using the DnrK (PDB code: 9LA8) structure as the search model, likewise, the structure of DnrK^{E299A}-**5**-SAH was solved by molecular replacement, using the DnrK^{E299A} (PDB code: 9LAC) structure as the search model. Further manual model building was facilitated by using Coot,[47] combined with the structure refinement using Phenix.[48] Data collection and structure refinement statistics are summarized in Table S2. The Ramachandran statistics, as calculated by Molprobity,[49] are 98.36%/0.75%, 98.95%/0.38% (favored/outliers) for structures of DnrK and DnrK^{E299A}, respectively. All the structural diagrams were prepared using the program ChimeraX 1.6.1.[50]

Molecular Docking of Substrate 1 to DnrK

To place the substrate into the active site of the DnrK, molecular docking of substrate **1** with DnrK was performed using Autodock vina 1.2.0,[51] resulting in protein−substrate complex structures. Chem3D 19.0 was used to generate ligand **1**. The final structure of DnrK bound with **1** was selected based on the binding state of **3** in the DnrK co-crystal structure in this paper. After the protein−substrate complex structure were prepared, the substrate−protein interactions were analyzed using PLIP (the protein−ligand interaction profiler) (https://plip-tool.biotec.tu-dresden.de) to determine key catalytic residues. ChimeraX 1.6.1 was used for viewing the molecular interactions and image processing.

Isotopic Labeling Experiments

To further verify the catalytic mechanism of DnrK, ^{18}O labeling water (≥98% labeled, Tenglong Weibo, Qingdao) and $^{18}O_2$ (≥98% labeled, Delin, Shanghai) were used to replace water or O_2 in the reaction system.

For $^{18}O_2$ labeling experiments, the reaction was performed in a 100 μL reaction buffer (H_2O) using a liquid bottle (2 mL). 2 μM DnrK or DnrK^{E299} each mutant was added to the reaction system, respectively. Then the bottle was purged with nitrogen and sealed with a liquid bottle cap. $^{18}O_2$ was introduced into the bottle from the compressed gas bag via a syringe needle. Finally, 100 μM **1** was added to the bottle using a microsyringe. After incubation for each enzyme at 30 °C for 60 min, 100 μL methanol was added to terminated the reactions.

For $H_2{}^{18}O$ labeling experiments, the enzymatic reactions of 2 μM DnrK or its mutants with 100 μM **1** were performed in a 100 μL reaction buffer ($H_2{}^{18}O$) using a microcentrifuge tube (1.5 mL). After incubation at 30 °C for 2 h, 100 μL of methanol was added to quenched the reaction. LC-HRMS analysis was carried out using the same method above.

Protein Conformation Analysis Using Circular Dichroism Spectrum (CD)

Protein samples were diluted to a final concentration of 0.15 mg/mL using the buffer containing 50 mM NaH_2PO_4, and the CD spectra were collected in the wavelength range of 190−280 nm with a step size of 0.5 nm at 25 °C using a 200 μL cuvette. The buffer containing 50 mM NaH_2PO_4 was served as the background control, and its spectrum was subtracted from each sample spectrum.

The Antiproliferative Activity Screening

The antiproliferative effects of compounds **2**−**5** were assessed by using the Cell Counting Kit 8 (CCK-8) assay.[52−54] Specifically, the cells were suspended in culture medium supplemented with 10% fetal bovine serum and inoculated into 96-well plates at a density of 5×10^4 cells/mL for adherent cells and 9×10^4 cells/mL for suspension cells, with 90 μL per well. The plates were incubated at 37 °C with 5% CO_2 for 24 h. Subsequently, 10 μL of sample solution was added to each well for IC_{50} determination, and eight concentration gradients were tested with three replicates per concentration. The plates were

https://doi.org/10.1021/acscatal.5c07819
ACS Catal. 2026, 16, 3522−3533

incubated for an additional 48 h. The experiment was divided into a blank group, a control group, and a drug group. After incubation, the old culture medium and drug solution were removed from the adherent cells. Then 100 μL of CCK-8 solution (diluted 10-fold in the basic medium) was added and the suspension cells was directly added 10 μL of CCK-8 stock solution. The plates were incubated for 1−4 h at 37 °C with 5% CO_2 (dark operation, real-time observation). Absorbance was measured at 450 nm using an enzyme-labeling instrument and the original data and results were recorded. The toxicity was quantified by cell inhibition percentage, calculated as $(OD_{Control} - OD_{Drug})/(OD_{Control} - OD_{Blank}) \times 100\%$. The IC_{50} values were determined using GraphPad Prism9.5 software, and the results are presented as the mean ± SD. Doxorubicin hydrochloride served as the positive control.

■ ASSOCIATED CONTENT

Supporting Information

The Supporting Information is available free of charge at https://pubs.acs.org/doi/10.1021/acscatal.5c07819.

Primers; details of X-ray data collection and refinement statistics; antiproliferative activity data; multiple sequence alignments of relevant methyltransferases; SDS-PAGEs gel analyses for all proteins; investigations with SAM analogues; circular dichroism analysis; LC-HRMS data; NMR spectra; and additional figures (PDF)

■ AUTHOR INFORMATION

Corresponding Author

Wei Zhang − *Laboratory of Experimental Marine Biology, Institute of Oceanology, Chinese Academy of Sciences, Qingdao 266000, China; State Key Laboratory of Microbial Technology, Shandong University, Qingdao, Shandong 266237, China; Laboratory for Marine Biology and Biotechnology, Qingdao Marine Science and Technology Center, Qingdao, Shandong 266237, China; Shenzhen Research Institute of Shandong University, Shenzhen 518057, China;* orcid.org/0000-0001-9459-680X; Email: weizhang@qdio.ac.cn

Authors

Moli Sang − *Laboratory of Experimental Marine Biology, Institute of Oceanology, Chinese Academy of Sciences, Qingdao 266000, China; State Key Laboratory of Microbial Technology, Shandong University, Qingdao, Shandong 266237, China*

Qingyu Yang − *Laboratory of Experimental Marine Biology, Institute of Oceanology, Chinese Academy of Sciences, Qingdao 266000, China; State Key Laboratory of Microbial Technology, Shandong University, Qingdao, Shandong 266237, China*

Jiawei Guo − *State Key Laboratory of Microbial Technology, Shandong University, Qingdao, Shandong 266237, China*

Peiyuan Feng − *Laboratory of Experimental Marine Biology, Institute of Oceanology, Chinese Academy of Sciences, Qingdao 266000, China*

Yu Gao − *Laboratory of Experimental Marine Biology, Institute of Oceanology, Chinese Academy of Sciences, Qingdao 266000, China*

Wencheng Ma − *Laboratory of Experimental Marine Biology, Institute of Oceanology, Chinese Academy of Sciences, Qingdao 266000, China; State Key Laboratory of Microbial Technology, Shandong University, Qingdao, Shandong 266237, China*

Shengying Li − *State Key Laboratory of Microbial Technology, Shandong University, Qingdao, Shandong 266237, China;* orcid.org/0000-0002-5244-870X

Mikko Metsä-Ketelä − *Department of Life Technologies, University of Turku, FIN-20014 Turku, Finland;* orcid.org/0000-0003-3176-2908

Complete contact information is available at: https://pubs.acs.org/10.1021/acscatal.5c07819

Notes

The authors declare no competing financial interest.

■ ACKNOWLEDGMENTS

This work was supported by the National Natural Science Foundation of China (Nos. U2106227 and 82022066), the Independent Deployment Project of the Institute of Oceanology, Chinese Academy of Sciences (No. IOCASZZCG009), the Postdoctoral Science Foundation of China (No. 2025M772727), and the Shenzhen Fundamental Research Program (No. JCYJ20220530141208018). We are grateful to Prof. Wenjun Guan (Zhejiang University) for generously providing the *S. coeruleorubidus* strain. We also thank the staff of the Institute of Oceanology, Chinese Academy of Sciences and the Core Facilities for Life and Environmental Sciences, State Key Laboratory of Microbial Technology of Shandong University for the LC-HRMS and NMR analyses.

■ REFERENCES

(1) Aubel-Sadron, G.; Londos-Gagliardi, D. Daunorubicin and doxorubicin, anthracycline antibiotics, a physicochemical and biological review. *Biochimie* **1984**, *66* (5), 333−352.

(2) Cersosimo, R. J.; Hong, W. K. Epirubicin: a review of the pharmacology, clinical activity, and adverse effects of an adriamycin analogue. *J. Clin. Oncol.* **1986**, *4* (3), 425−439.

(3) Warrell, R. P., Jr. Aclacinomycin A: clinical development of a novel anthracycline antibiotic in the haematological cancers. *Drugs Exp. Clin. Res.* **1986**, *12* (1−3), 275−282.

(4) Krohn, K. *Anthracycline Chemistry and Biology I: Biological Occurrence and Biosynthesis, Synthesis and Chemistry*, 1st ed.; Springer: Heidelberg, 2009; Vol. *282*.

(5) Hulst, M. B.; Grocholski, T.; Neefjes, J. J. C.; van Wezel, G. P.; Metsä-Ketelä, M. Anthracyclines: biosynthesis, engineering and clinical applications. *Nat. Prod. Rep.* **2022**, *39* (4), 814−841.

(6) Hortobagyi, G. N. Anthracyclines in the treatment of cancer. An overview. *Drugs* **1997**, *54 Suppl*, 1−7.

(7) Gao, Q.; Deng, S.; Jiang, T. Recent developments in the identification and biosynthesis of antitumor drugs derived from microorganisms. *Eng. Microbiol.* **2022**, *2* (4), No. 100047.

(8) Martins-Teixeira, M. B.; Carvalho, I. Antitumour anthracyclines: progress and perspectives. *ChemMedChem.* **2020**, *15* (11), 933−948.

(9) Najafi, M.; Hooshangi Shayesteh, M. R.; Mortezaee, K.; Farhood, B.; Haghi-Aminjan, H. The role of melatonin on doxorubicin-induced cardiotoxicity: a systematic review. *Life Sci.* **2020**, *241*, No. 117173.

(10) Hertweck, C.; Luzhetskyy, A.; Rebets, Y.; Bechthold, A. Type II polyketide synthases: gaining a deeper insight into enzymatic teamwork. *Nat. Prod. Rep.* **2007**, *24* (1), 162−190.

(11) Grocholski, T.; Dinis, P.; Niiranen, L.; Niemi, J.; Metsä-Ketelä, M. Divergent evolution of an atypical *S*-adenosyl-L-methionine−dependent monooxygenase involved in anthracycline biosynthesis. *Proc. Natl. Acad. Sci. U. S. A.* **2015**, *112* (32), 9866−9871.

(12) Dinis, P.; Tirkkonen, H.; Wandi, B. N.; Siitonen, V.; Niemi, J.; Grocholski, T.; Metsä-Ketelä, M. Evolution-inspired engineering of anthracycline methyltransferases. *Proc. Natl. Acad. Sci. Nexus.* **2023**, *2* (2), 1−10.

(13) Jansson, A.; Niemi, J.; Lindqvist, Y.; Mäntsälä, P.; Schneider, G. Crystal structure of aclacinomycin-10-hydroxylase, a *S*-adenosyl-L-methionine-dependent methyltransferase homolog involved in anthracycline biosynthesis in *Streptomyces purpurascens*. *J. Mol. Biol.* **2003**, *334* (2), 269−280.
(14) Jansson, A.; Koskiniemi, H.; Mäntsälä, P.; Niemi, J.; Schneider, G. Crystal structure of a ternary complex of DnrK, a methyltransferase in daunorubicin biosynthesis, with bound products. *J. Biol. Chem.* **2004**, *279* (39), 41149−41156.
(15) Wang, Y. L.; Niemi, J.; Mäntsälä, P. Modification of aklavinone and aclacinomycins in vitro and *in vivo* by rhodomycin biosynthesis gene products. *FEMS Microbiol. Lett.* **2002**, *208* (1), 117−122.
(16) Jansson, A.; Koskiniemi, H.; Erola, A.; Wang, J.; Mantsala, P.; Schneider, G.; Niemi, J. Aclacinomycin 10-hydroxylase is a novel substrate-assisted hydroxylase requiring *S*-adenosyl-L-methionine as cofactor. *J. Biol. Chem.* **2005**, *280* (5), 3636−3644.
(17) Sang, M. L.; Yang, Q. Y.; Guo, J. W.; Feng, P. Y.; Ma, W. C.; Zhang, W. Functional investigation of the SAM-dependent methyltransferase RdmB in anthracycline biosynthesis. *Synth. Syst. Biotechnol.* **2025**, *10* (1), 102−109.
(18) Blumauerová, M.; Matějů, J.; Stajner, K.; Vaněk, M. Z. Studies on the production of daunomycinone derived glycosides and related metabolites in *Streptomyces coeruleorubidus* and *Streptomyces peucetius*. *Folia Microbiol.* **1977**, *22* (4), 275−285.
(19) Martin, J. L.; McMillan, F. M. SAM (dependent) I AM: The *S*-adenosylmethionine-dependent methyltransferase fold. *Curr. Opin. Struct. Biol.* **2002**, *12* (6), 783−793.
(20) Liscombe, D. K.; Louie, G. V.; Noel, J. P. Architectures, mechanisms and molecular evolution of natural product methyltransferases. *Nat. Prod. Rep.* **2012**, *29* (10), 1238−1250.
(21) Struck, A. W.; Thompson, M. L.; Wong, L. S.; Micklefield, J. *S*-adenosyl-methionine-dependent methyltransferases: highly versatile enzymes in biocatalysis, biosynthesis and other biotechnological applications. *ChemBioChem.* **2012**, *13* (18), 2642−2655.
(22) O'Hagan, D.; Schmidberger, J. W. Enzymes that catalyse S_N2 reaction mechanisms. *Nat. Prod. Rep.* **2010**, *27* (6), 900−918.
(23) Abdelraheem, E.; Thair, B.; Varela, R. F.; Jockmann, E.; Popadic, D.; Hailes, H. C.; Ward, J. M.; Iribarren, A. M.; Lewkowicz, E. S.; Andexer, J. N.; Hagedoorn, P. L.; Hanefeld, U. Methyltransferases: functions and applications. *ChemBioChem* **2022**, *23* (18), No. e202200212.
(24) Coward, J. K.; Slisz, E. P. Analogs of *S*-adenosylhomocysteine as potential inhibitors of biological transmethylation. Specificity of the *S*-adenosylhomocysteine binding site. *J. Med. Chem.* **1973**, *16* (5), 460−463.
(25) Borchardt, R. T.; Eiden, L. E.; Wu, B.; Rutledge, C. O. Sinefungin, a potent inhibitor or *S*-adenosylmethionine: protein *O*-methyltransferase. *Biochem. Biophys. Res. Commun.* **1979**, *89* (3), 919−924.
(26) Fetzner, S.; Steiner, R. A. Cofactor-independent oxidases and oxygenases. *Appl. Microbiol. Biotechnol.* **2010**, *86* (3), 791−804.
(27) Grocholski, T.; Koskiniemi, H.; Lindqvist, Y.; Mäntsälä, P.; Niemi, J.; Schneider, G. Crystal structure of the cofactor-independent monooxygenase SnoaB from *Streptomyces nogalater*: implications for the reaction mechanism. *Biochemistry* **2010**, *49* (5), 934−944.
(28) Wang, Q. Q.; Qiao, Y.; Wei, D. Unraveling proton-coupled electron transfer in cofactor-free oxidase-and oxygenase-catalyzed oxygen activation: a theoretical view. *Phys. Chem. Chem. Phys.* **2024**, *27* (1), 20−31.
(29) Thierbach, S.; Bui, N.; Zapp, J.; Chhabra, S. R.; Kappl, R.; Fetzner, S. Substrate-assisted O_2 activation in a cofactor-independent dioxygenase. *Chem. Biol.* **2014**, *21* (2), 217−225.
(30) Widboom, P. F.; Fielding, E. N.; Liu, Y.; Bruner, S. D. Structural basis for cofactor-independent dioxygenation in vancomycin biosynthesis. *Nature* **2007**, *447* (7142), 342−345.
(31) Steiner, R. A.; Janssen, H. J.; Roversi, P.; Oakley, A. J.; Fetzner, S. Structural basis for cofactor-independent dioxygenation of *N*-heteroaromatic compounds at the alpha/beta-hydrolase fold. *Proc. Natl. Acad. Sci. U. S. A.* **2010**, *107* (2), 657−662.
(32) Dickens, M. L.; Priestley, N. D.; Strohl, W. R. *In vivo* and *in vitro* bioconversion of epsilon-rhodomycinone glycoside to doxorubicin: functions of DauP, DauK, and DoxA. *J. Bacteriol.* **1997**, *179* (8), 2641−2650.
(33) Grocholski, T.; Yamada, K.; Sinkkonen, J.; Tirkkonen, H.; Niemi, J.; Metsä-Ketelä, M. Evolutionary trajectories for the functional diversification of anthracycline methyltransferases. *ACS Chem. Biol.* **2019**, *14* (5), 850−856.
(34) Jin, W. B.; Wu, S.; Jian, X. H.; Yuan, H.; Tang, G. L. A radical-adenosyl-L-methionine enzyme and a methyltransferase catalyze cyclopropane formation in natural product biosynthesis. *Nat. Commun.* **2018**, *9* (1), 2771−2781.
(35) Ohashi, M.; Liu, F.; Hai, Y.; Chen, M. B.; Tang, M. C.; Yang, Z. Y.; Sato, M.; Watanabe, K.; Houk, K. N.; Tang, Y. SAM-dependent enzyme-catalysed pericyclic reactions in natural product biosynthesis. *Nature* **2017**, *549* (7673), 502−506.
(36) Chang, Z. Y.; Ansbacher, T.; Zhang, L. L.; Yang, Y.; Ko, T. P.; Zhang, G. M.; Liu, W. D.; Huang, J. W.; Dai, L. H.; Guo, R. T.; Major, D. T.; Chen, C. C. Crystal structure of LepI, a multifunctional SAM-dependent enzyme which catalyzes pericyclic reactions in leporin biosynthesis. *Org. Biomol. Chem.* **2019**, *17* (8), 2070−2076.
(37) Gui, C.; Kalkreuter, E.; Liu, Y. C.; Li, G. N.; Steele, A. D.; Yang, D.; Chang, C. S.; Shen, B. Cofactorless oxygenases guide anthraquinone-fused enediyne biosynthesis. *Nat. Chem. Biol.* **2024**, *20* (2), 243−250.
(38) Jiang, C.; Qi, Z.; Kang, Q.; Liu, J.; Jiang, M.; Bai, L. Formation of the Δ (18,19) double bond and bis(spiroacetal) in salinomycin is atypically catalyzed by SlnM, a methyltransferase-like enzyme. *Angew. Chem., Int. Ed. Engl.* **2015**, *54* (31), 9097−9100.
(39) Fage, C. D.; Isiorho, E. A.; Liu, Y.; Wagner, D. T.; Liu, H. W.; Keatinge-Clay, A. T. The structure of SpnF, a standalone enzyme that catalyzes [4 + 2] cycloaddition. *Nat. Chem. Biol.* **2015**, *11* (4), 256−258.
(40) Zhao, Y.; Liu, X.; Xiao, Z.; Zhou, J.; Song, X.; Wang, X.; Hu, L.; Wang, Y.; Sun, P.; Wang, W.; et al. *O*-methyltransferase-like enzyme catalyzed diazo installation in polyketide biosynthesis. *Nat. Commun.* **2023**, *14* (1), 5372−5385.
(41) Ohashi, M.; Jamieson, C. S.; Cai, Y.; Tan, D.; Kanayama, D.; Tang, M. C.; Anthony, S. M.; Chari, J. V.; Barber, J. S.; Picazo, E.; Kakule, T. B.; Cao, S.; Garg, N. K.; Zhou, J.; Houk, K. N.; Tang, Y. An enzymatic Alder-ene reaction. *Nature* **2020**, *586* (7827), 64−69.
(42) Notredame, C.; Higgins, D. G.; Heringa, J. T-Coffee: A novel method for fast and accurate multiple sequence alignment. *J. Mol. Boil.* **2000**, *302* (1), 205−217.
(43) Robert, X.; Gouet, P. Deciphering key features in protein structures with the new ENDscript server. *Nucleic Acids Res.* **2014**, *42* (W1), W320−W324.
(44) Blin, K.; Shaw, S.; Kloosterman, A. M.; Charlop-Powers, Z.; van Wezel, G. P.; Medema, M. H.; Weber, T. antiSMASH 6.0: improving cluster detection and comparison capabilities. *Nucleic Acids Res.* **2021**, *49* (W1), W29−W35.
(45) Minor, W.; Cymborowski, M.; Otwinowski, Z.; Chruszcz, M. HKL-3000: the integration of data reduction and structure solution−from diffraction images to an initial model in minutes. *Acta Crystallogr., D: Biol. Crystallogr.* **2006**, *62* (8), 859−866.
(46) McCoy, A. J.; Grosse-Kunstleve, R. W.; Adams, P. D.; Winn, M. D.; Storoni, L. C.; Read, R. J. Phaser crystallographic software. *J. Appl. Crystallogr.* **2007**, *40* (4), 658−674.
(47) Emsley, P.; Cowtan, K. Coot: model-building tools for molecular graphics. *Acta Crystallogr.* **2004**, *60* (12), 2126−2132.
(48) Adams, P. D.; Afonine, P. V.; Bunkóczi, G.; Chen, V. B.; Davis, I. W.; Echols, N.; Headd, J. J.; Hung, L. W.; Kapral, G. J.; Grosse-Kunstleve, R. W.; McCoy, A. J.; Moriarty, N. W.; Oeffner, R.; Read, R. J.; Richardson, D. C.; Richardson, J. S.; Terwilliger, T. C.; Zwart, P. H. PHENIX: a comprehensive Python-based system for macromolecular structure solution. *Acta Crystallogr., Sect. D: Biol. Crystallogr.* **2010**, *66* (2), 213−221.
(49) Davis, I. W.; Leaver-Fay, A.; Chen, V. B.; Block, J. N.; Kapral, G. J.; Wang, X.; Murray, L. W.; Arendall, W. B., III; Snoeyink, J.;

https://doi.org/10.1021/acscatal.5c07819
ACS Catal. 2026, 16, 3522−3533

Richardson, J. S.; Richardson, D. C. MolProbity: all-atom contacts and structure validation for proteins and nucleic acids. *Nucleic Acids Res.* **2007**, *35*, W375−W383.
(50) Pettersen, E. F.; Goddard, T. D.; Huang, C. C.; Meng, E. C.; Couch, G. S.; Croll, T. I.; Morris, J. H.; Ferrin, T. E. UCSF ChimeraX: Structure visualization for researchers, educators, and developers. *Protein Sci.* **2021**, *30* (1), 70−82.
(51) Morris, G. M.; Huey, R.; Lindstrom, W.; Sanner, M. F.; Belew, R. K.; Goodsell, D. S.; Olson, A. J. AutoDock4 and AutoDockTools4: Automated docking with selective receptor flexibility. *J. Comput. Chem.* **2009**, *30* (16), 2785−2791.
(52) Tominaga, H.; Ishiyama, M.; Ohseto, F.; Sasamoto, K.; Hamamoto, T.; Suzuki, K.; Watanabe, M. A water-soluble tetrazolium salt useful for colorimetric cell viability assay. *Anal. Commun.* **1999**, *36* (2), 47−50.
(53) Liu, X. Y.; Wei, W.; Wang, C. L.; Yue, H.; Ma, D.; Zhu, C.; Ma, G. H.; Du, Y. G. Apoferritin-camouflaged Pt nanoparticles: surface effects on cellular uptake and cytotoxicity. *J. Mater. Chem.* **2011**, *21* (20), 7105−7110.
(54) Xu, M. Y.; Lee, S. Y.; Kang, S. S.; Kim, Y. S. Antitumor activity of jujuboside B and the underlying mechanism via induction of apoptosis and autophagy. *J. Nat. Prod.* **2014**, *77* (2), 370−376.

https://doi.org/10.1021/acscatal.5c07819
ACS Catal. 2026, 16, 3522−3533